Figure 4

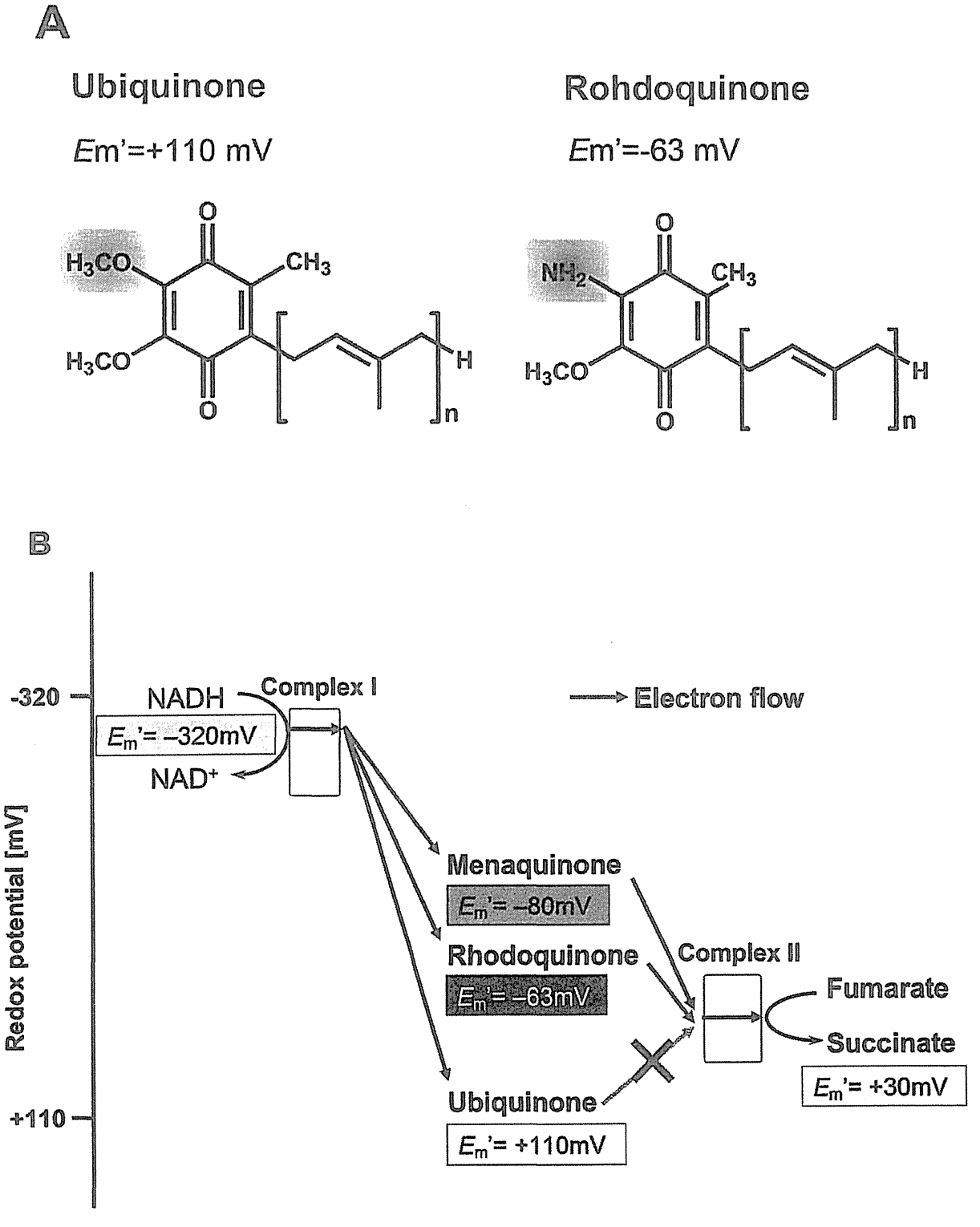
A
Ubiquinone
Em'=+110 mV
Rohdoquinone
Em'=-63 mV
B
-320
+110
Redox potential [mV]
NADH
Em'= –320mV
NAD+
Complex I
Electron flow
Menaquinone
Em'= –80mV
Rhodoquinone
Em'= –63mV
Ubiquinone
Em'= +110mV
Complex II
Fumarate
Succinate
Em'= +30mV

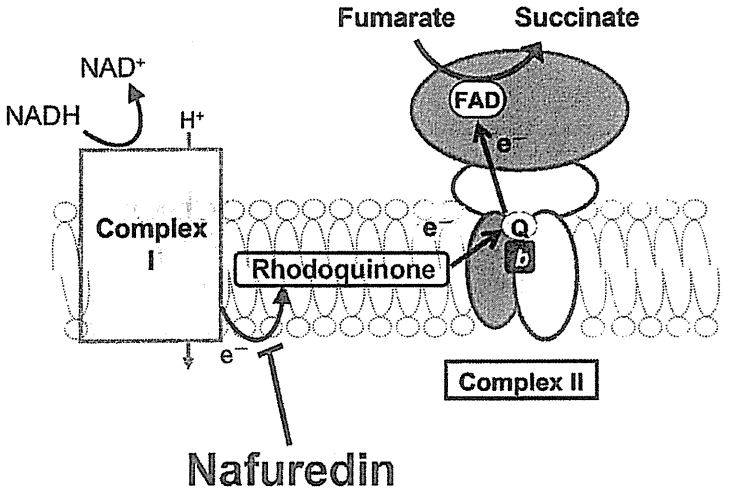
Fumarate
Succinate
NAD+
NADH
H+
FAD
e−
Complex I
e−
Q
b
Rhodoquinone
e−
Complex II
Nafuredin

Figure 5

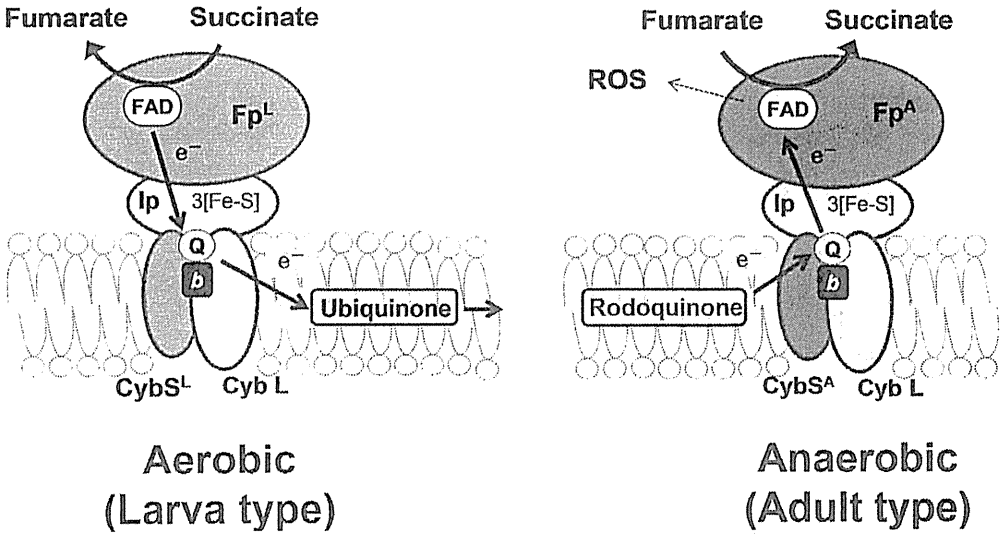
Fumarate
Succinate
FAD
Fp^L
e⁻
Ip
3[Fe-S]
Q
b
e⁻
Ubiquinone
CybS^L
Cyb L
Aerobic
(Larva type)
Fumarate
Succinate
ROS
FAD
Fp^A
e⁻
Ip
3[Fe-S]
Q
e⁻
Rodoquinone
b
CybS^A
Cyb L
Anaerobic
(Adult type)

Figure 6

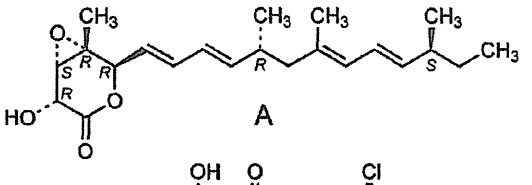
CH3
CH3
CH3
CH3
CH3
O
R
S
R
R
R
S
HO
O
O
A

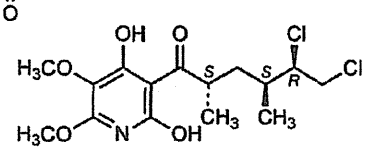
OH
O
Cl
H3CO
S
S
R
Cl
CH3
CH3
H3CO
N
OH
B

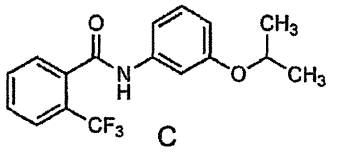
O
CH3
N
H
O
CH3
CF3
C

Figure 7

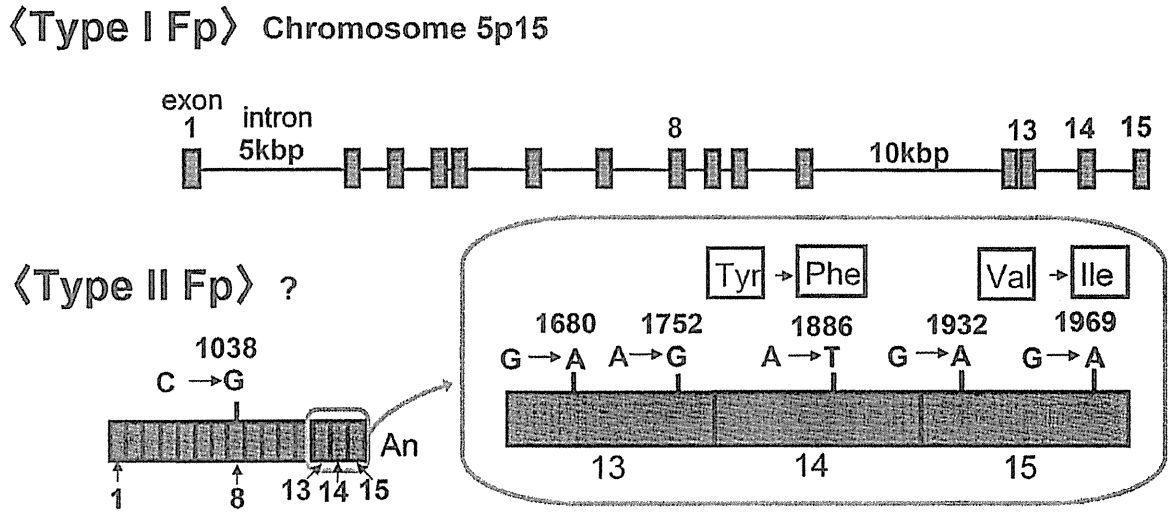
〈Type I Fp〉 Chromosome 5p15
exon
1
intron
5kbp
8
10kbp
13
14
15
〈Type II Fp〉 ?
1038
C →G
An
1
8
13 14 15
Tyr → Phe
Val → Ile
1680
1752
1886
1932
1969
G →A
A →G
A →T
G →A
G →A
13
14
15

Figure 8

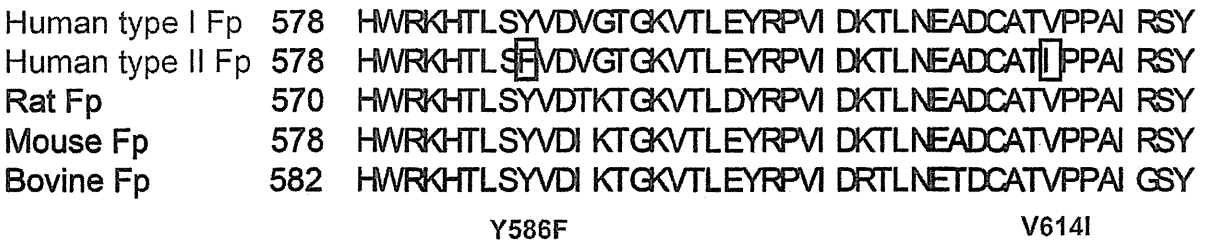
Human type I Fp 578 HWRKHTLSYVDVGTGKVTLEYRPVI DKTLNEADCATVPPAI RSY
Human type II Fp 578 HWRKHTLSFVDVGTGKVTLEYRPVI DKTLNEADCATIPPAI RSY
Rat Fp 570 HWRKHTLSYVDTKTGKVTLDYRPVI DKTLNEADCATVPPAI RSY
Mouse Fp 578 HWRKHTLSYVDIKTGKVTLEYRPVI DKTLNEADCATVPPAI RSY
Bovine Fp 582 HWRKHTLSYVDIKTGKVTLEYRPVI DRTLNETDCATVPPAI GSY
Y586F
V614I

Figure 9

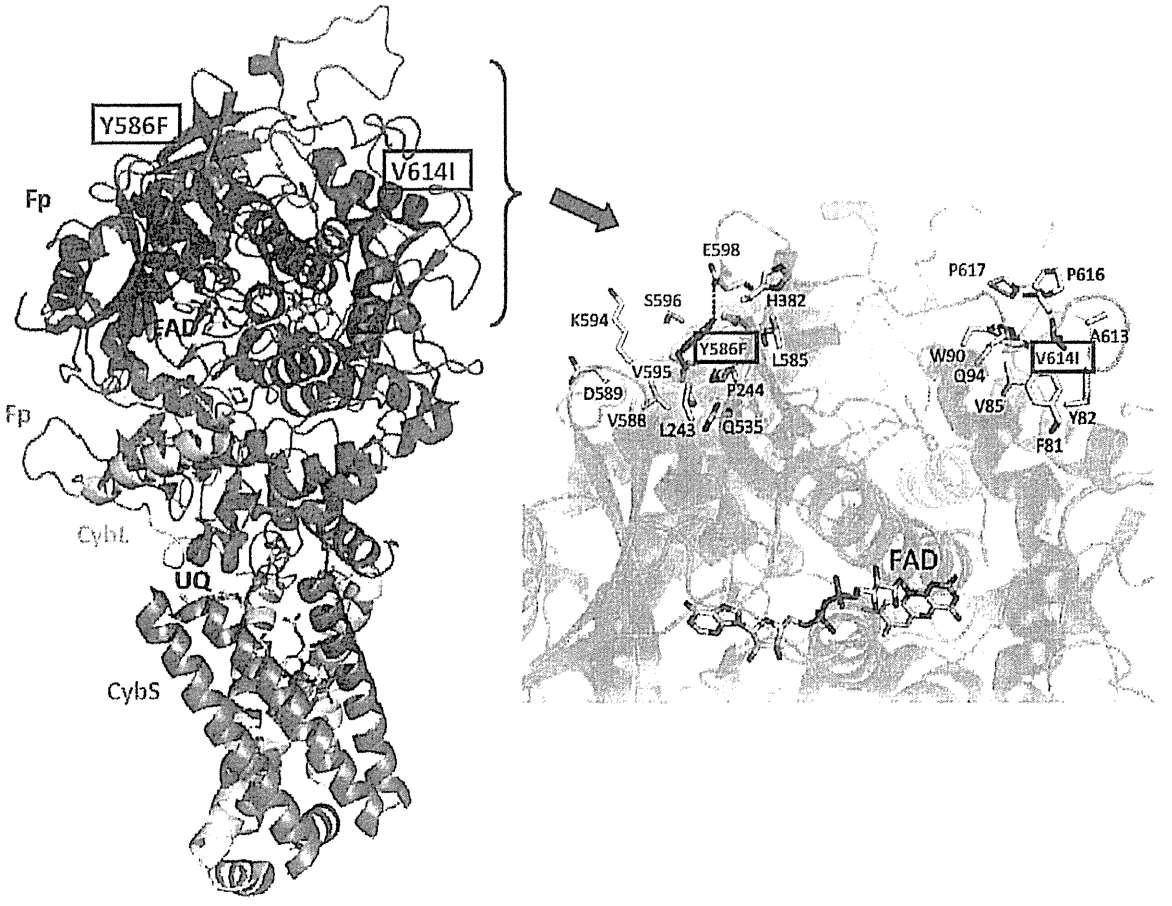
Y586F
V614I
Fp
FAD
Fp
CybL
UQ
CybS
E598
S596
H382
K594
Y586F
L585
V595
P244
D589
V588
L243
Q535
P617
P616
A613
W90
V614I
Q94
V85
Y82
F81
FAD

Figure 10

Author's Choice

THE JOURNAL OF BIOLOGICAL CHEMISTRY VOL. 287, NO. 20, pp. 16379–16389, May 11, 2012

Muscle-specific Knock-out of NUAK Family SNF1-like Kinase 1 (NUAK1) Prevents High Fat Diet-induced Glucose Intolerance*[S]

Received for publication, September 13, 2011, and in revised form, March 9, 2012 Published, JBC Papers in Press, March 14, 2012, DOI 10.1074/jbc.M111.302687

Fumika Inazuka[‡§], Naoyuki Sugiyama[¶], Masaru Tomita[¶], Takaya Abe[‖], Go Shioi[‖], and Hiroyasu Esumi[‡§1]

From the [‡]Department of Integrated Biosciences, Graduate School of Frontier Sciences, The University of Tokyo, Kashiwa 277-8561, Japan, the [§]Cancer Physiology Project, Research Center for Innovative Oncology, National Cancer Center Hospital East, Kashiwa 277-8577, Japan, the [¶]Institute for Advanced Biosciences, Keio University, Tsuruoka 997-0017, Japan, and the [‖]Laboratory for Animal Resources and Genetic Engineering, RIKEN Center for Developmental Biology, Kobe, 650-0047, Japan

Background: The physiological roles of NUAK1 are poorly understood because of embryonic lethality in NUAK1 null mice.
Results: Negative feedback regulation of insulin signaling was abrogated in skeletal muscle of muscle-specific NUAK1 knock-out mice.
Conclusion: NUAK1 controls glucose metabolism through negative regulation of insulin signal transduction in skeletal muscle.
Significance: This is the first report of a physiological role of NUAK1 in adult tissues.

NUAK1 is a member of the AMP-activated protein kinase-related kinase family. Recent studies have shown that NUAK1 is involved in cellular senescence and motility in epithelial cells and fibroblasts. However, the physiological roles of NUAK1 are poorly understood because of embryonic lethality in NUAK1 null mice. The purpose of this study was to elucidate the roles of NUAK1 in adult tissues. We determined the tissue distribution of NUAK1 and generated muscle-specific NUAK1 knock-out (MNUAK1KO) mice. For phenotypic analysis, whole body glucose homeostasis and muscle glucose metabolism were examined. Quantitative phosphoproteome analysis of soleus muscle was performed to understand the molecular mechanisms underlying the knock-out phenotype. Nuak1 mRNA was preferentially expressed in highly oxidative tissues such as brain, heart, and soleus muscle. On a high fat diet, MNUAK1KO mice had a lower fasting blood glucose level, greater glucose tolerance, higher insulin sensitivity, and higher concentration of muscle glycogen than control mice. Phosphoproteome analysis revealed that phosphorylation of IRS1 Ser-1097 was markedly decreased in NUAK1-deficient muscle. Consistent with this, insulin signaling was enhanced in the soleus muscle of MNUAK1KO mice, as evidenced by increased phosphorylation of IRS1 Tyr-608, AKT Thr-308, and TBC1D4 Thr-649. These observations suggest that a physiological role of NUAK1 is to suppress glucose uptake through negative regulation of insulin signaling in oxidative muscle.

NUAK1 is a serine/threonine kinase belonging to the AMP-activated protein kinase-related kinase (AMPK-RK)[2] family. AMPK is a heterotrimer composed of an α catalytic subunit and two regulatory subunits: β and γ. The AMPK-RK family includes 12 proteins classified together on the basis of sequence similarity with AMPKαs (1, 2). The phosphorylation and activation of AMPKαs are up-regulated by AMP through binding to the γ regulatory subunit (3). On the other hand, AMPK-RKs do not have regulatory subunits; thus their activities are not directly regulated by the cellular AMP:ATP ratio (4). Like the AMPKαs and most other AMPK-RKs, NUAK1 can be phosphorylated by liver kinase B1 (LKB1) at a conserved threonine residue (corresponding to Thr-211 in NUAK1) (2). In addition to Thr-211, NUAK1 can be phosphorylated at Ser-600 by AKT (5). However, a recent study demonstrated that amino acid substitution at this site (S600A) has no influence on kinase activity (6). Thus, the functional significance of phosphorylation at Ser-600 is controversial.

In epithelial cells and fibroblasts, LKB1-NUAK1 phosphorylates myosin phosphatase target subunit 1 and large tumor suppressor homolog 1, which results in cell detachment and senescence, respectively (6, 7). NUAK1 also acts as a transcriptional coactivator in complex with LKB1 and tumor suppressor p53 to induce cell cycle G_1 arrest in A549 lung adenocarcinoma cells (8). In mouse C2C12 myoblasts, NUAK1 is increasingly expressed with differentiation to myotubes (9). Apart from these *in vitro* studies, a study involving knock-out mice showed that the mouse homolog of NUAK1 (OMPHK1) is essential for closure of the ventral body wall in developing embryos (10).

* This work was supported in part by a Grant for the 3rd Term Comprehensive 10-Year Strategy for Cancer Control from the Ministry of Health, Labour and Welfare Japan.
Author's Choice—Final version full access.
[S] This article contains supplemental text, references, mass spectra, and Tables S1–S3.
[1] To whom correspondence should be addressed: Cancer Physiology Project, Research Center for Innovative Oncology, National Cancer Center Hospital East, 6-5-1 Kashiwanoha, Kashiwa, Chiba 277-8577, Japan. Tel.: 81-4-7134-8786; Fax: 81-4-7134-8786; E-mail: hesumi@ncc.go.jp.

[2] The abbreviations used are: AMPK, AMP-activated protein kinase; AMPK-RK, AMPK-related kinase; IRS1, insulin receptor substrate 1; NUAK1, NUAK family SNF1-like kinase 1; TBC1D4, TBC1 domain family member 4; PGC-1α, peroxisome proliferator-activated receptor γ coactivator 1-α; TNNC, troponin C; GLUT4, glucose transporter type 4; GYS1, glycogen synthase 1; TA, tibialis anterior; EDL, extensor digitorum longus; OGTT, oral glucose tolerance test; ITT, insulin tolerance test; NC, normal chow diet; HFD, high fat diet; LKB, liver kinase B1; KHB, Krebs-Henseleit buffer; FDG, fluoro-D-glucose.

In a study with colorectal cancer clinical samples, increased NUAK1 mRNA has been observed (11). Overall, the functions and roles of NUAK1 have been investigated in the context of motility or proliferation of cultured cells, embryonic development, and cancer progression. However, little research has focused on the physiological roles of NUAK1 in adult tissues.

Skeletal muscle is the major tissue responsible for disposal of total body glucose (12). The two major physiological stimulators of skeletal muscle glucose uptake are insulin and muscle contraction (13). Contraction-stimulated glucose uptake has been shown to be mediated by LKB1 via AMPKα2 and/or NUAK2, an AMPK-RK with the highest homology to NUAK1 (14–20). In addition to the influences on contraction-stimulated glucose uptake, muscle-specific LKB1 knock-out mice display increased insulin sensitivity and improved whole body glucose homeostasis (21). In contrast, muscle-specific inhibition of AMPKα2 impairs insulin sensitivity and glucose tolerance (22). Other than AMPKα2 and NUAK2, little is known about the involvement of other AMPK-RKs in muscle glucose metabolism.

The purpose of this study was to elucidate the physiological roles of NUAK1 in adult tissues. For this purpose, we generated muscle-specific NUAK1 knock-out (MNUAK1KO) mice. To our knowledge, this is the first report of conditional knock-out of NUAK1. MNUAK1KO mice were apparently normal but exhibited improved glucose homeostasis under high fat diet (HFD) conditions. To understand the molecular mechanisms underlying the phenotype associated with the knock-out, we performed a quantitative phosphoproteome analysis of skeletal muscle. Our data suggest that one role of NUAK1 is suppression of insulin signal transduction in skeletal muscle.

EXPERIMENTAL PROCEDURES

Animal Protocols—All of the experimental protocols were approved by the Institutional Ethics Review Committee at the National Cancer Center. The mice were maintained on a 12-h light/dark cycle and housed in a temperature-controlled barrier facility with free access to water and a standard rodent chow composed of 20% calories from fat, 50% calories from carbohydrate, and 30% calories from protein (CMF; Oriental Yeast, Tokyo, Japan). *Nuak1*$^{flox/flox}$ mice were obtained from the Laboratory for Animal Resources and Genetic Engineering, Center for Developmental Biology, RIKEN Kobe (accession number CDB0555K). Prior to initiation of the present study, *Nuak1*$^{flox/flox}$ mice were backcrossed onto a C57BL/6J background using the speed cogenic method (Oriental Bioservice, Tokyo, Japan). To generate MNUAK1KO mice, *Nuak1*$^{flox/flox}$ mice were mated with muscle creatin kinase (*Mck*)-*Cre* mice (JAX, number 006475: B6.FVB (129S4)-Tg (Ckmm-cre) 5 Khn/J). As a control for MNUAK1KO mice, their *Nuak1*$^{flox/flox}$ littermate mice were used. For HFD-induced glucose intolerance, the mice were fed a HFD composed of 57% calories from fat, 23% calories from carbohydrate, and 20% calories from protein (HFD32; Clea Japan, Tokyo, Japan) starting from 5 weeks of age until the termination of the experiments. Male mice were used for all of the experiments.

Genotyping—Genomic DNA from various tissues was subjected to PCR involving 34 cycles of denaturation at 94 °C for 30 s, annealing at 60 °C for 30 s, and elongation at 72 °C for 90 s with the following primers: 5′-specific primer P1 (5′-GGTAGGTGGAGGTCGGCTGAGAAGG) and 3′-specific primer P2 (5′-TCGGATCCTAGTGAACCTCTTC).

Real Time RT-PCR—Total RNA was extracted using Isogen (Nippon Gene, Tokyo, Japan) and quantified using a NanoDrop 2000 spectrophotometer (Thermo Fisher Scientific, Waltham, MA). Equal amounts (3.5 μg/15-μl reaction) of total RNA were subjected to first strand cDNA synthesis using a first strand cDNA synthesis kit (GE Healthcare Japan) according to the manufacturer's instructions. Real time PCR was carried out with TaqMan Universal PCR Master Mix (Invitrogen Japan) and TaqMan gene expression assays (Invitrogen Japan) according to the manufacturer's protocols. The TaqMan gene expression assays used in this study were Nuak1 (Mm01250701_m1), Nuak2 (Mm00546961_m1), PGC-1α (Mm_01208835_m1), TNNC1 (Mm00437111_m1), TNNC2 (Mm00437116_m1), and 18 S rRNA (4319413E). For relative quantification, C_t values for each gene were normalized to those for 18 S rRNA. For absolute quantification, synthesized oligonucleotide DNA fragments (Sigma-Aldrich Japan) containing the PCR amplicon regions were used to generate standard curves.

Immunoblotting—Following sacrifice, mouse tissues were rapidly dissected and frozen in liquid nitrogen. The frozen samples were homogenized in lysis buffer containing 1% SDS, 10 mM Tris (pH 7.5), 1 mM Na_3VO_4, and protease inhibitor mixture (Sigma-Aldrich Japan) and then subjected to SDS-PAGE. The proteins were transferred onto a polyvinylidene fluoride microporous membrane (Millipore, MA). The primary antibodies used were: anti-NUAK1 (4458), anti-phospho-LKB1 Ser-428 (3482), anti-LKB1 (3047), anti-IRS1 (2382), anti-phospho-AKT Thr-308 (9275), and anti-AKT (4685), all obtained from Cell Signaling Technologies (Beverly, MA), anti-phospho-TBC1D4 Thr-642 (ab65753), and anti-glucose transporter type 4 (GLUT4) (ab65976), obtained from Abcam (Cambridge, UK), anti-TBC1D4 (07-741) and anti-phospho-IRS1 Tyr-608 (09-432), obtained from Millipore (Billerica, MA), and anti-actin (sc-1615), obtained from Santa Cruz Biotechnology (Santa Cruz, CA). Immunoblots were scanned using a Canoscan LiDE60 image scanner (Cannon, Tokyo, Japan), and the intensities of the protein bands were quantified using an image processing program ImageJ 1.44.

Measurements of Blood Glucose, Insulin, and Muscle Glycogen—Blood glucose levels were measured from tail blood using an Antsense II glucometer (Bayer Medical, Tokyo, Japan). Plasma insulin levels were determined from peripheral blood using mouse insulin ELISA kit S-Type (Shibayagi, Gunma, Japan). The glycogen concentration of the soleus muscle was determined using a glycogen assay kit (BioVision, Milpitas, CA). For oral glucose tolerance tests (OGTT), mice fasted overnight were administered glucose at a dose of 1 g/kg of body weight. Blood glucose levels were measured immediately before and 20, 40, 60, and 120 min after the administration. For insulin tolerance tests (ITT), mice fasted for 2 h were injected intraperitoneally with recombinant human insulin (Wako Pure Chemical Industries, Osaka, Japan) at a dose of 1 unit/kg of

body weight. Blood glucose levels were measured immediately before and 15, 30, and 60 min after the injection.

Histological Analysis—Soleus muscles were fixed with 10% neutral buffered formalin, embedded in paraffin, and sectioned at 6-μm thickness. The sections were stained using Alexa Fluor 555-conjugated wheat germ agglutinin and Hoechst 33342 (Invitrogen Japan). The immunofluorescent images were visualized with a Zeiss LSM 710 confocal laser microscope (Carl Zeiss Japan). The myocyte cross-sectional areas obtained from 84 cells from six control mice and 83 cells from six MNUAK1KO mice were quantified by ZEN 2009 image viewer software (Carl Zeiss Japan).

Measurements of Glucose Uptake in Skeletal Muscles—All of the incubation media were pregassed with 95% O_2, 5% CO_2, and all incubation was performed at 30 °C. *Ex vivo* muscle incubation was performed as described previously (23). Soleus muscles were incubated for 30 min in Krebs-Henseleit buffer (KHB) (pH 7.4) containing 10 mM HEPES, 5.5 mM glucose, 2 mM pyruvate, and 0.05% free fatty acid free-bovine serum albumin without or with insulin (20 milliunits/ml). Subsequently, the muscles were washed with glucose-free KHB without or with insulin (20 milliunits/ml) three times. Glucose transport was then determined in KHB supplemented with 0.5 MBq/ml 2-deoxy-2-[^{18}F]fluoro-D-glucose ([^{18}F]FDG) (Nihon Medi-Physics, Tokyo, Japan), 0.75 mM FDG, and 9 μM mannitol in the absence or presence of insulin (20 milliunits/ml) for 20 min. [^{18}F]FDG was washed out with ice-cold KHB without glucose and without insulin three times. Thereafter, the muscles were blotted and weighed. The remaining radioactivity derived from [^{18}F]FDG was measured by a Wizard 2 automatic γ-counter (PerkinElmer Japan).

Phosphoproteome Analysis—Soleus muscles were frozen in liquid nitrogen and disrupted using a multibead shocker (MB400U; Yasui Kikai, Osaka, Japan). Homogenates of the muscles were reduced with dithiothreitol and then alkylated with iodoacetamide before being subjected to a dual enzymatic digestion (Lys-C followed by trypsin) (24). Digested samples were desalted using StageTips with SDB-XC Empore disk membranes (3M Company, St. Paul, MN) (25). Dimethyl labeling was performed according to the literature (26). Phosphopeptide enrichment based on hydroxy acid-modified metal oxide chromatography was performed using lactic acid-modified titania as described previously with a slight modification (27). The eluates from hydroxy acid-modified metal oxide chromatography were concentrated in a vacuum evaporator (CC-105; Tomy, Tokyo, Japan). NanoLC-MS/MS analysis was performed using a previously described setup (28). Peptides and proteins were identified by Mascot version 2.3 (Matrix Science, Tokyo, Japan) against the Uniprot/SwissProt data base release 2011_04 with a precursor mass tolerance of 3 ppm, a fragment ion mass tolerance of 0.8 Da, and strict trypsin specificity allowing for up to two missed cleavages. Cysteine carbamidomethylation was set as a fixed modification. Oxidation of methionine, phosphorylation of serine, threonine, and tyrosine, and [$^{1}H_4$,$^{12}C_2$/$^{2}H_4$,$^{13}C_2$]dimethylation of the N terminus and lysine were allowed as variable modifications. Peptides were considered identified if the Mascot score was over the 95% confidence limit based on the "identity" score of each peptide, and at least three successive y or b ions and two or more y, b, and/or precursor origin neutral loss ions were observed, based on the error-tolerant peptide sequence tag concept (29). False positive rates were estimated by searching against a randomized decoy data base created by the Mascot Perl program supplied by Matrix Science (averaged false positive rate = 1.02%). The details of experimental procedures are described in the supplemental information.

RESULTS

NUAK1 Is Preferentially Expressed in Highly Oxidative Tissues Such as Cerebrum, Heart, and Soleus Muscle—To determine the tissue distribution of NUAK1, the level of mouse Nuak1 mRNA in various organs and tissues was measured using quantitative RT-PCR. The distribution of Nuak2 mRNA was also examined because NUAK1 and NUAK2 may have redundant functions (7, 30). As shown in Fig. 1*A*, Nuak1 was most abundant in the cerebrum and heart, which is consistent with the distribution of human NUAK1 (31). We found that among the skeletal muscles examined, Nuak1 was selectively expressed in the soleus, at a level comparable with the heart. In contrast, Nuak2 was barely detectable in the skeletal muscles and was highly expressed in kidney.

Expression of NUAK1 protein in the heart, soleus, tibialis anterior (TA), and extensor digitorum longus (EDL) muscles was analyzed using immunoblotting, which also showed muscle type-specific expression of NUAK1 (Fig. 1*B*). LKB1 was expressed in all of the muscles examined, and the phosphorylation level was lower in the heart than in the other muscles (Fig. 1*B*). Previous studies have shown that soleus muscle predominantly contains type I and type IIA fibers, which have a high mitochondrial density and oxidative capacity (32). Therefore, our data suggest that NUAK1 is preferentially expressed in highly oxidative tissues such as the cerebrum, heart, and soleus muscle.

Generation of MNUAK1KO Mice—To investigate the role of NUAK1 in skeletal muscle, we generated conditional knockout (MNUAK1KO) mice. Mice carrying Nuak1 floxed allele (*Nuak1$^{flox/flox}$*), in which exon 3 was flanked by *loxP* sequences as shown in Fig. 1*C*, were crossed with muscle creatin kinase (*Mck*)-*Cre* transgenic mice. The MNUAK1KO mice were born in a normal Mendelian ratio and had no gross abnormalities in appearance and behavior. Genomic PCR analysis confirmed deletion of the Nuak1 gene in the heart and skeletal muscles of MNUAK1KO mice. The deletion was not observed in any non-muscle tissues in the MNUAK1KO mice or in tissues from their *Nuak1$^{flox/flox}$* (control) littermates (Fig. 1*D*). Real time RT-PCR showed that the level of Nuak1 mRNA was substantially reduced in heart, soleus, TA, and EDL muscles of MNUAK1KO mice (Fig. 1*E*). The NUAK1 protein was barely detectable in those tissues of MNUAK1KO mice (Fig. 1*F*). These observations confirmed that muscle-specific knock-out of NUAK1 was achieved.

MNUAK1KO Mice Exhibit No Skeletal Muscle Morphological Abnormalities—For phenotypic analysis, we first assessed the mass and fiber size of the soleus muscle, as well as the weight of heart and body, because the involvement of NUAK1 in myoblast differentiation has been implied (9). No difference was

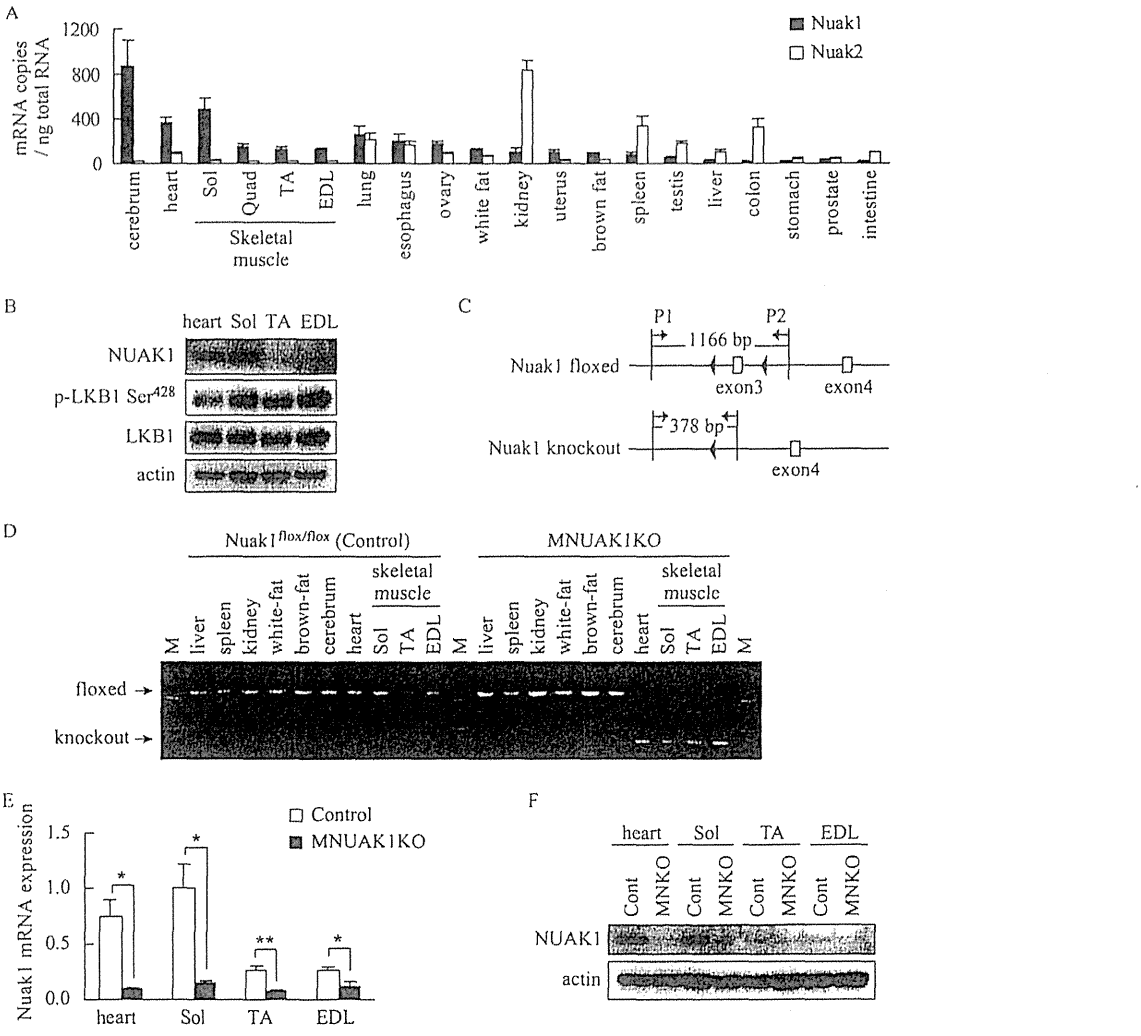

FIGURE 1. **NUAK1 is preferentially expressed in highly oxidative tissues.** *A*, quantitative RT-PCR analysis of Nuak1 and Nuak2. RNA was isolated from 10-week-old C57BL/6 mice. The data are the means ± S.E. ($n = 3$). *B*, immunoblotting analysis of NUAK1 and LKB1 in heart, Sol, TA, and EDL muscles. Actin was used as a loading control. Protein extracts were from three individual 10-week-old C57BL/6 mice. *C*, schematic representation of floxed and knock-out alleles of Nuak1. The *black arrowheads* represent *loxP* sites. *Gray arrows* indicate PCR primers P1 and P2 used for the genotyping. Amplification with the P1 and P2 primers yields the 1166-bp product from the floxed allele and the 378-bp product from the knock-out allele. *D*, genotyping of Nuak1 floxed mice without (control) or with (MNUAK1KO) the *Mck-Cre* transgene. *M*, molecular marker. *E*, real time RT-PCR for Nuak1 mRNA in muscles. RNA was isolated from 10-week-old control and MNUAK1KO mice. The mRNA levels are expressed relative to that in soleus muscle of control mice. The data are the means ± S.E. ($n = 3$). *, $p < 0.05$; **, $p < 0.01$ (Student's *t* test). *F*, immunoblot analysis of NUAK1 protein in muscles. Protein extracts of each type of muscle were prepared from three individual mice. *Sol*, soleus; *Quad*, quadriceps; *Cont*, control; *MNKO*, MNUAK1KO.

observed between MNUAK1KO and control mice with respect to body, heart, or soleus weights under both normal chow diet (NC) and HFD conditions at 13–15 weeks of age (Fig. 2, *A* and *B*, and supplemental Table S1). The myocyte cross-sectional area of the soleus muscle was almost identical in MNUAK1KO and control mice (Fig. 2*C*). The expression of NUAK1 in heart or soleus muscle of control mice was not affected by the HFD (data not shown).

To determine whether NUAK1 is involved in the formation of type I fibers, we examined the expression level of peroxisome proliferator-activated receptor γ coactivator 1-α (PGC-1α), a transcriptional regulator that drives type I fiber formation (33). We also assessed myofiber composition by examining the expression levels of troponin C1 (TNNC1) and troponin C2 (TNNC2), which are specifically expressed in type I and type II fibers, respectively (32). Real time RT-PCR analysis revealed no significant difference between MNUAK1KO and control mice with respect to PGC-1α, TNNC1, or TNNC2 mRNA expression in the soleus, TA, and EDL muscles (Fig. 2, *D–F*). These observations suggest that NUAK1 is not involved in the determination of muscle mass, fiber size, or fiber type.

MNUAK1KO Mice Fed High Fat Diet Exhibit Improved Glucose Homeostasis—To assess the influence of muscle-specific knock-out of NUAK1 on whole body glucose homeostasis, MNUAK1KO and control mice were fed either a NC or a HFD, and the level of blood glucose was monitored. There was no difference in the fasting blood glucose concentration of MNUAK1KO and control mice fed a NC through age 19 weeks (Fig. 3, *A* and *B*). In contrast, on a HFD, the fasting blood glucose concentration at 13–15 weeks of age was significantly lower in MNUAK1KO mice than in control mice (Fig. 3*A*). This phenotype was even more prominent by age 18–19 weeks (Fig. 3*B*). At this age, MNUAK1KO mice fed a HFD exhibited slightly lower body weight compared with that of control mice

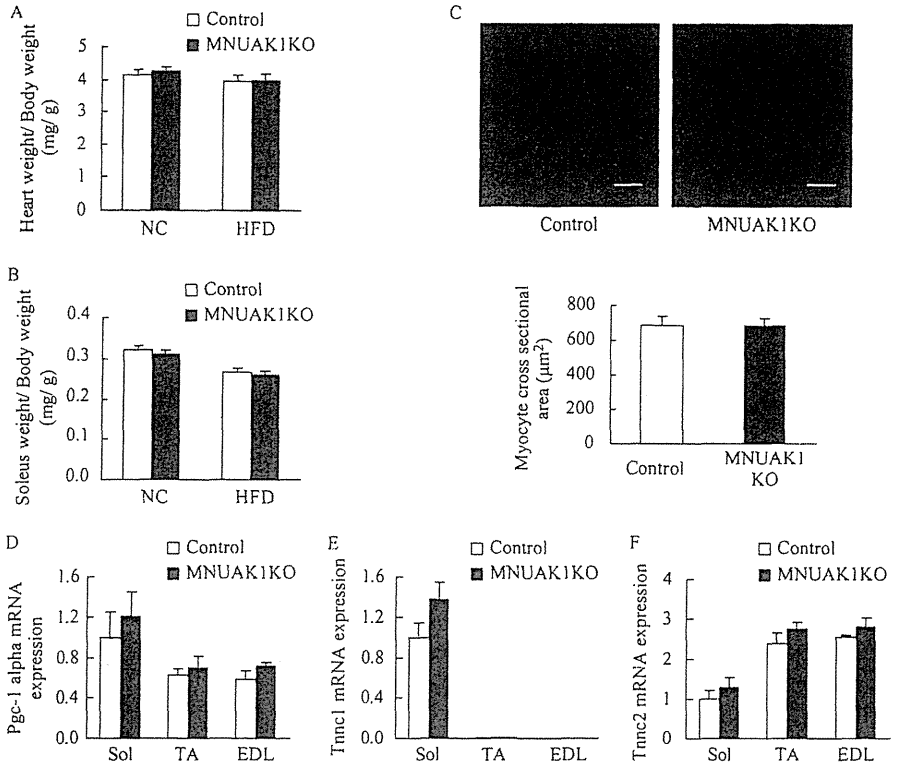

FIGURE 2. **MNUAK1KO mice display no morphological abnormalities.** *A* and *B*, weight of heart (*A*) and soleus muscle (*B*) of control and MNUAK1KO mice fed a NC or HFD. The indicated values are normalized to body weight. The data are the means ± S.E. (n = 10). *C*, cross-section of soleus muscle myocytes stained with wheat germ agglutinin. *Scale bars*, 20 μm. The graph below shows the average myocyte cross-sectional area for control and MNUAK1KO mice. The data are the means ± S.E. (n = 6). *D–F*, real time RT-PCR analysis of PGC-1α (*D*), TNNC1 (*E*), and TNNC2 (*F*). The mRNA levels are expressed relative to that of the soleus in control mice. The data are the means ± S.E. (n = 3). Mice at the age of 13–15 weeks were used for all experiments. *Sol*, soleus.

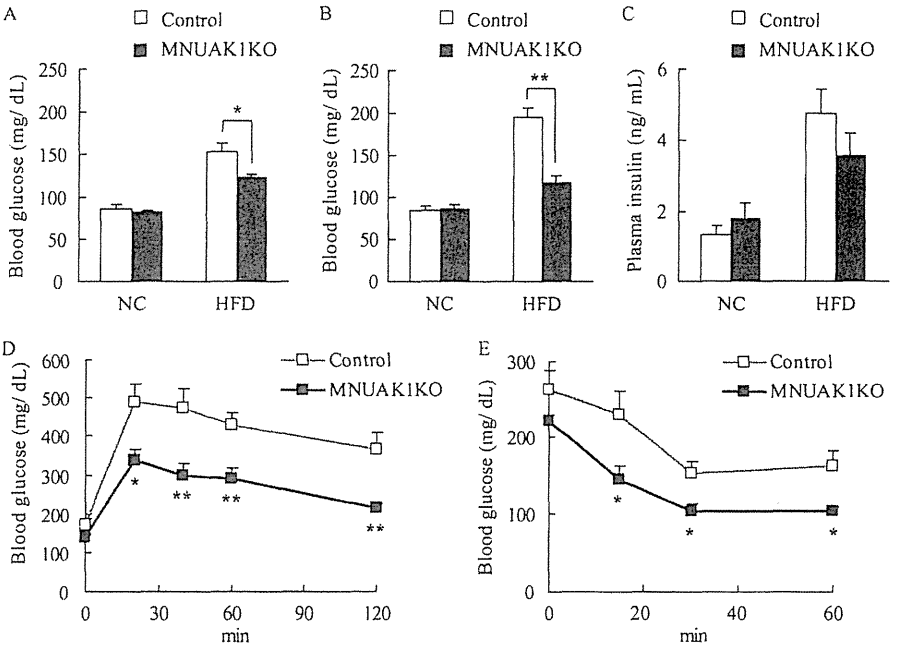

FIGURE 3. **MNUAK1KO mice show improved glucose homeostasis under HFD conditions.** *A* and *B*, fasting blood glucose levels of control and MNUAK1KO mice at 13–15 weeks (*A*) and 18–19 weeks of age (*B*). The data are the means ± S.E. (n = 8). *C*, plasma insulin levels of control and MNUAK1KO mice. The data are the means ± S.E. (n = 12). *D*, oral glucose tolerance of control and MNUAK1KO mice under HFD conditions. The data are the means ± S.E. (n = 12). *E*, insulin tolerance of control and NUAK1 KO mice under HFD conditions. The data are the means ± S.E. (n = 8). Mice at the age of 13–15 weeks were used for *C–E*. *, $p < 0.05$; **, $p < 0.01$ (Student's t test).

(supplemental Table S1), which may reflect the improved glucose homeostasis in MNUAK1KO mice. In conjunction with these findings, the fasting plasma free fatty acid level was significantly lower in MNUAK1KO mice than in control mice under HFD conditions (supplemental Table S1). The HFD-induced hyperinsulinemia and hypertriglyceridemia also tended

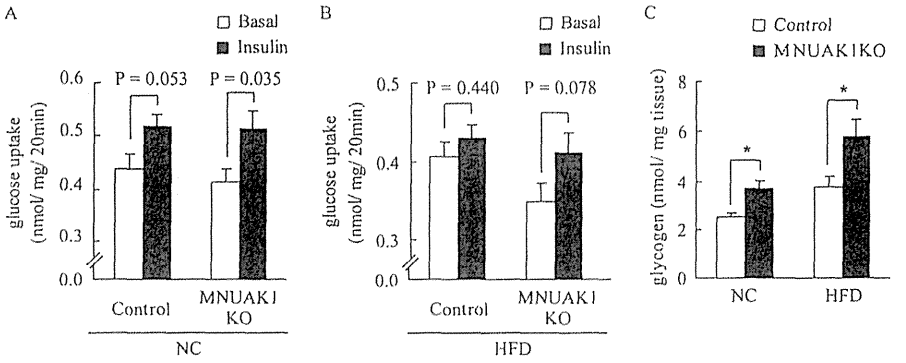

FIGURE 4. **MNUAK1KO mice show improved insulin sensitivity and increased glycogen storage in skeletal muscle.** *A* and *B*, rate of glucose uptake in soleus muscles isolated from 18–20-week-old control and MNUAK1KO mice fed a NC (*A*) or a HFD (*B*) without or with insulin stimulation. The data are the means ± S.E. ($n = 7$ for NC and 8 for HFD). *C*, glycogen concentration in the soleus muscle of 13–15-week-old control and MNUAK1KO mice fed a NC or HFD. The data are the means ± S.E. ($n = 8$). *, $p < 0.05$ (Student's *t* test).

to be less pronounced in MNUAK1KO mice (Fig. 3*C* and supplemental Table S1). The level of food intake was unaltered between MNUAK1KO and control mice (supplemental Table S1).

To further investigate the involvement of NUAK1 in glucose homeostasis, an oral glucose tolerance test (OGTT) and an insulin tolerance test (ITT) were performed. No differences in OGTT and ITT results were observed between MNUAK1KO and control mice fed a NC (data not shown). On a HFD, MNUAK1KO mice displayed significantly lower blood glucose levels than control mice as determined using both the OGTT (Fig. 3*D*) and the ITT (Fig. 3*E*). These results indicate that muscle-specific knock-out of NUAK1 increases the capacity for glucose disposal, at least in part, in response to insulin.

To determine whether the improved whole body glucose metabolism is attributed to NUAK1-deficient skeletal muscle, we measured glucose uptake into isolated soleus muscle without or with insulin. Insulin-stimulated glucose uptake was observed in the soleus muscle from both MNUAK1 and control mice fed a NC (Fig. 4*A*). Under HFD conditions, the effects of insulin were less pronounced in the soleus muscle from control mice, whereas NUAK1-deficient soleus muscle displayed insulin-stimulated glucose uptake comparable with that observed under NC conditions (Fig. 4*B*). We also measured the soleus muscle glycogen concentration in MNUAK1KO and control mice. The glycogen concentration was significantly higher in the soleus of MNUAK1KO mice under both NC and HFD conditions, indicating that NUAK1 plays a critical role in glucose storage in the soleus muscle (Fig. 4*C*). Taken together, our findings suggest that a muscle-specific knock-out of NUAK1 preserved insulin sensitivity under HFD conditions.

Phosphorylation of TBC1D4 Is Increased by Deletion of Nuak1 in Skeletal Muscle—Glucose metabolism in skeletal muscle is highly sensitive to both the expression of glucose transporter type 4 (GLUT4) which is increased by exercise and decreased by a HFD (34, 35), and its translocation to the plasma membrane (36–38), which is facilitated by phosphorylated TBC1 domain family member 4 (TBC1D4) (39, 40). To investigate the molecular mechanism underlying improved glucose metabolism, the TBC1D4 phosphorylation in acute response to glucose in the soleus of HFD-fed MNUAK1KO and control mice was examined. The level of GLUT4 protein was also

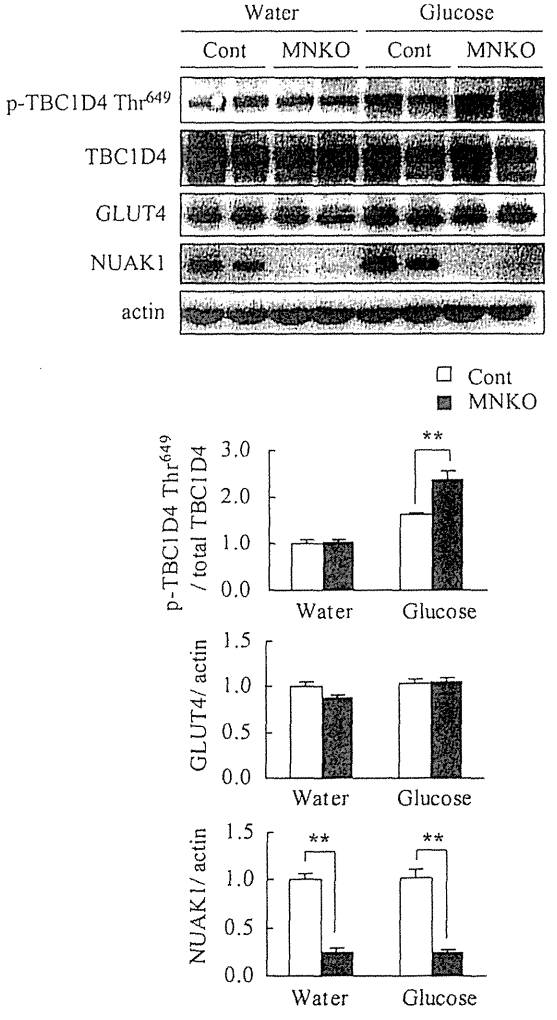

FIGURE 5. **Phosphorylation of TBC1D4 is up-regulated in NUAK1-deficient muscle after glucose administration.** Immunoblot analysis of TBC1D4, GLUT4, and NUAK1 in soleus muscle of HFD-fed control and MNUAK1KO mice. Mice at the age of 13–15 weeks were fasted overnight and sacrificed 40 min after oral administration of water (basal control) or glucose. The graphs show the intensities of phospho-TBC1D4, GLUT4, and NUAK1 bands. Phospho-TBC1D4 protein levels were normalized to total TBC1D4. GLUT4 and NUAK1 protein levels were normalized to actin. The protein levels are expressed relative to those in the water-administered control mice. The data are the means ± S.E. ($n = 4$ for NUAK1 and 5 for TBC1D4 and GLUT4). **, $p < 0.01$ (Student's *t* test). *Cont*, control; *MNKO*, MNUAK1KO.

TABLE 1

Phosphoproteome analysis in soleus muscles from MNUAK1KO and control mice fed a HFD

The listed phosphorylation sites were differentially regulated more than 2.0-fold in MNUAK1KO mice compared with control mice under HFD conditions. The data are means ± S.E. ($n = 4$).

Symbol	Name	Potential phosphorylation-sites in unique peptides	KO/Control ratio
Phosphoproteins decreased in MNUAK1KO			
Glucose metabolism			
PKCtheta	Protein kinase C theta type	S676[b]	**0.40** ± 0.13
IRS1	Insulin receptor substrate 1	S1097[b]	**0.10** ± 0.03
GYS1	Glycogen [starch] synthase, muscle	S652, S657[b]	**0.42** ± 0.04
		S653[b], S657[b]	**0.50** ± 0.05
Actin-myosin cytoskeleton			
MYH1/ 4/ 6/ 7/ 8[a]	Myosin-1/ 4/ 6/ 7/ 8	S1044/ S1041/ S1039/ S1037/ S1040	**0.33** ± 0.09
TTN	Titin	S322	**0.47** ± 0.07
		S2078, S2080	**0.48** ± 0.07
TCAP	Telethonin	S39	**0.47** ± 0.07
CTNNA1	Catenin alpha-1	S641[b]	**0.30** ± 0.09
SYNPO2L	Synaptopodin 2-like protein	T138, S140	**0.40** ± 0.07
CMYA5	Cardiomyopathy-associated protein 5	S769	**0.37** ± 0.06
PLEC	Plectin	S4629, Y4618 or Y4619 or S4620[c]	**0.27** ± 0.03
		S4392, S4393, S4396	**0.34** ± 0.04
		S4620, S4633	**0.37** ± 0.08
		Y4622, S4629	**0.37** ± 0.08
		Y4622, S4627	**0.42** ± 0.05
		Y4619, S4627	**0.42** ± 0.06
		Y4622, T4630	**0.44** ± 0.01
		S4392, S4393	**0.48** ± 0.05
		Y4622, S4625	**0.49** ± 0.03
Protein biosynthesis			
EIF5B	Eukaryotic translation initiation factor 5B	S108, S114	**0.34** ± 0.07
RPLP2	60S acidic ribosomal protein P2	S105[b]	**0.34** ± 0.03
DNAJC1	DnaJ homolog subfamily C member 1	S477, S478	**0.41** ± 0.04
Miscellaneous			
LNP	Protein lunapark	S411	**0.35** ± 0.05
STEAP3	Metalloreductase STEAP3	S17, S20	**0.33** ± 0.04
GOGA4	Golgin subfamily A member 4	T39, S41	**0.41** 0.03
UBP2L	Ubiquitin-associated protein 2-like	S497, S480 or T481 or S482[c]	**0.31** ± 0.03
Phosphoproteins increased in MNUAK1KO			
Actin-myosin cytoskeleton			
LRRC39	Leucine-rich repeat-containing protein 39	S328	**2.20** ± 0.07
ANKRD2	Ankyrin repeat domain-containing protein 2	S347, T351	**3.63** ± 0.69
Protein biosynthesis			
EIF5B	Eukaryotic translation initiation factor 5B	S137	**4.23** 1.27
Miscellaneous			
HMGA1	High mobility group protein HMG-I/HMG-Y	S102, S103	**2.22** ± 0.46
PACSIN3	Protein kinase C and casein kinase II substrate protein 3	S354	**2.32** ± 0.32
2310046A06RIK	Uncharacterized protein C6orf142 homolog	S85	**2.01** ± 0.25

[a] Protein isoforms that could not be distinguished by unique peptides.
[b] Phosphorylation sites previously identified using site-specific methods in reference to the PhosphoSitePlus database.
[c] Ambiguous phosphorylation sites (*i.e.*, those that could not be determined from MS-MS spectra).

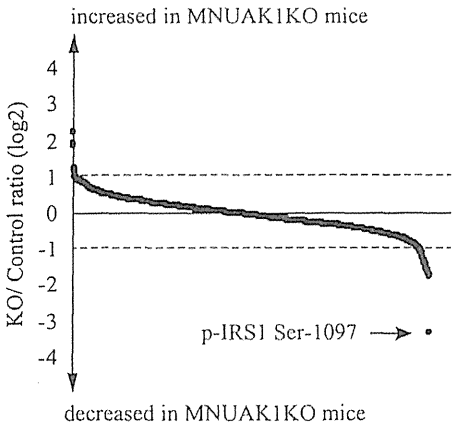

FIGURE 6. **Phosphoproteome of soleus muscles from MNUAK1KO and control mice.** A total of 1,229 phosphopeptides were quantitatively detected in soleus muscle. KO/control ratio of phosphopeptides are shown by *blue dots* (mean, $n = 4$). Phosphopeptides with KO/control ratio of more than 2.0 or less than 0.5 are listed in Table 1. An IRS1 phosphopeptide containing Ser-1097 is indicated by an *arrow*.

compared between MNUAK1KO and control mice. The phosphorylation level of TBC1D4 Thr-649 (corresponding to Thr-642 in the human isoform) was significantly higher in the soleus muscle from MNUAK1KO mice in the glucose-administered group (Fig. 5). This difference was not observed in the water-administered group, suggesting that postprandial glucose uptake is enhanced in the soleus of MNUAK1KO mice. No differences were observed in the GLUT4 protein level (Fig. 5). Our data indicate that the observed increase in glucose disposal in MNUAK1KO mice fed a HFD is associated with increased GLUT4 translocation rather than changes in GLUT4 expression in the soleus muscle.

Insulin Signal Transduction Is Enhanced in Soleus Muscle of MNUAK1KO Mice—To obtain a comprehensive understanding of the molecular mechanism underlying the observed MNUAK1KO phenotype, a quantitative phosphoproteome analysis was performed on soleus muscle isolated from HFD-fed MNUAK1KO and control mice in random fed state. Total protein was enzymatically digested, differentially labeled with stable isotopes, and then subjected to simultaneous LC-MS/MS analysis, which allowed for precise comparison between the two samples. To ensure reproducibility, four independent experiments were performed. All of the mass spectra and a detailed list of all proteins identified in this study are provided in the supplemental mass spectra and supplemental Table 3, respectively. Table 1 shows proteins that were found to be differentially phosphorylated more than 1.5-fold in all four experiments and more than 2-fold in average between MNUAK1KO and control mice. Among the 1,229 phosphopeptides quantitatively detected, the abundance of 27 phosphopeptides, corresponding to 21 proteins, decreased as a result of the Nuak1 deletion, whereas the abundance of six phosphopeptides, corresponding to six proteins, increased. Most of the differences in phosphorylation status were also observed under NC conditions (supplemental Table S2). It should be noted that differential regulation of phosphoproteins involved in glucose metabolism was clearly shown. In particular, the phosphorylation of IRS1 at Ser-1097 was changed most drastically (KO/control ratio = 0.10 ± 0.03) (Fig. 6). This serine phosphorylation (Ser-1101 in the human isoform), together with the phosphorylation of its upstream regulator PKCθ at Ser-676 (the same residue in the human isoform), is known to mediate negative feedback regulation of insulin signaling through blocking of IRS1 tyrosine phosphorylation (41). Phosphorylation of glycogen synthase 1 (GYS1) at the C-terminal serine residues including Ser-653 and Ser-657 (both same in the human isoform) leads to its inactivation and decreases glycogen synthesis (42, 43). Therefore, the hypophosphorylation of these sites in NUAK1-deficient soleus muscle can enhance insulin sensitivity and glycogen synthesis, which is consistent with the observed decreased blood glucose, improved glucose tolerance and insulin sensitivity, and increased muscle glycogen content phenotype. Besides glucose metabolism, biological processes shown to be affected include cell motility. Components of the actin-myosin cytoskeleton, such as various myosin isoforms, titin, and plectin, were also hypophosphorylated in NUAK1-deficient soleus muscle. Although it is unclear how changes in the phosphorylation status of these cytoskeletal proteins affect glucose metabolism and muscle contraction, the data suggest that NUAK1 has a role in regulation of muscle cytoskeletal structure.

To validate the increased insulin signaling suggested by the phosphoproteome analysis, phosphorylation of IRS1 at Tyr-608 and AKT at Thr-308 in soleus muscle of mice fed a HFD were analyzed by immunoblotting. The phosphorylation levels of IRS1 and AKT were significantly higher in soleus muscle of MNUAK1KO mice than in that of control mice under fed conditions, confirming the enhancement of insulin signaling by a lack of NUAK1 (Fig. 7*A*). We also examined the phosphorylation of IRS1 and AKT in acute response to glucose and insulin in soleus muscle of mice fed a HFD. As shown in Fig. 7*B*, phosphorylation levels of IRS1 Tyr-608 and AKT Thr-308 in response to glucose administration were significantly higher in soleus muscle of MNUAK1KO mice than in that of control mice. The AKT Thr-308 phosphorylation in response to insulin injection was also significantly higher in the soleus muscle of MNUAK1KO mice than in that of control mice (Fig. 7*C*). No difference was observed in IRS1 phosphorylation in response to insulin injection, probably because of the time point for this analysis. Note that phosphorylation level of AKT under basal (fasted) conditions was significantly lower in soleus muscle of MNUAK1KO mice than in that of control mice (Fig. 7, *B* and *C*). An increase in the basal phosphorylation level of AKT is characteristic of insulin resistance induced by a HFD (44, 45). These observations strongly suggest that a HFD-induced insulin resistance was reduced in soleus muscle of MNUAK1KO mice. Therefore, we concluded that NUAK1 is involved in the negative regulation of insulin signal transduction in soleus muscle.

DISCUSSION

Skeletal muscle is the principle tissue for insulin-mediated glucose uptake. Oxidative muscle has higher insulin-stimulated glucose transport activity than does glycolytic muscle (46). Therefore, our finding that NUAK1 is highly expressed in soleus muscle as well as cerebrum and heart, which are also highly oxidative tissues, suggests the possibility that NUAK1 is involved in energy metabolism in oxidative tis-

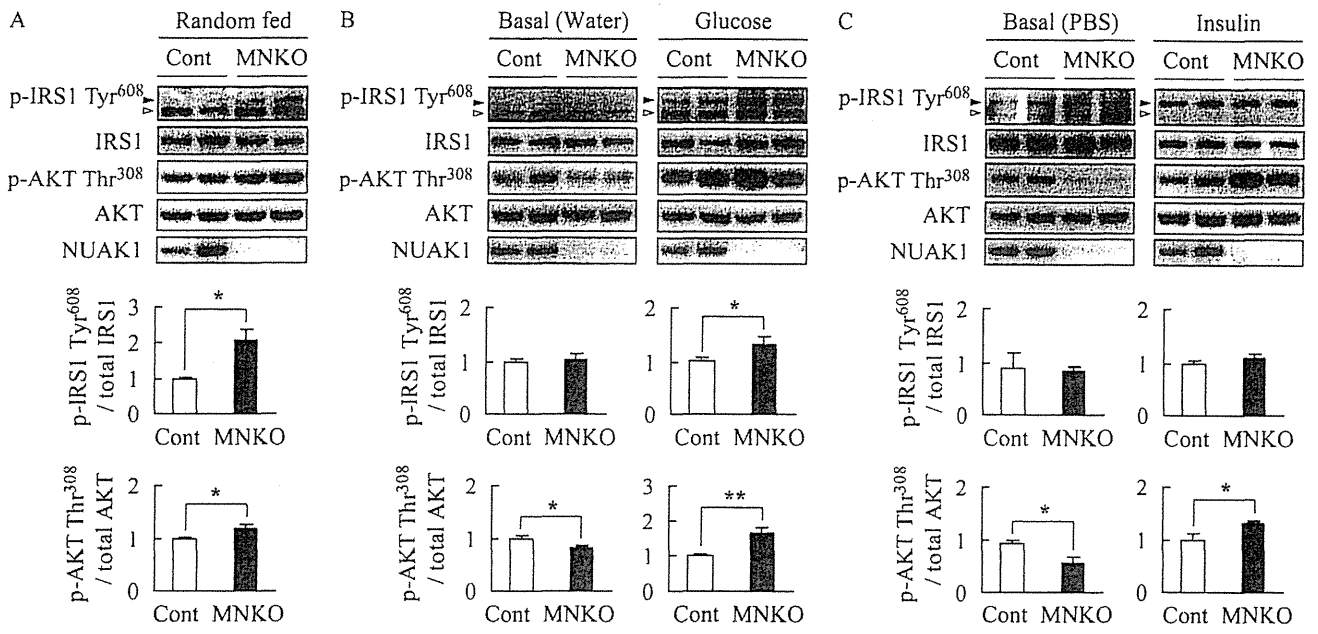

FIGURE 7. **Phosphorylation of insulin signaling proteins are up-regulated in NUAK1-deficient muscle.** Immunoblot analysis of phosphorylation of IRS1 at Tyr-608 (*black arrowhead*) and AKT at Thr-308 in soleus muscle of HFD-fed control and MNUAK1KO mice. A *white arrowhead* denotes a nonspecific band. Graphs show the intensities of phospho-protein bands normalized to total protein levels in each case. The data are expressed relative to those from control mice. *, $p < 0.05$; **, $p < 0.01$ (Student's *t* test). *A*, mice under fed conditions. The data are the means ± S.E. ($n = 3$). *B*, mice were fasted overnight and administered water or glucose (1 g/kg of body weight). Soleus was excised 40 min after the administration. The data are the means ± S.E. ($n = 6$). *C*, mice were fasted overnight and intraperitoneally injected with PBS or insulin (1.5 units/kg of body weight). Soleus was excised 20 min after the injection. The data are the means ± S.E. ($n = 3$). *Cont*, control; *MNKO*, MNUAK1KO.

sues. In support of this hypothesis, muscle-specific LKB1 knock-out (MLKB1KO) mice show improved whole body glucose homeostasis (21). Thus, we examined whether muscle-specific deletion of Nuak1 affects whole body glucose homeostasis and found that MNUAK1KO mice fed a HFD exhibit decreased fasting blood glucose levels and improved glucose metabolism compared with control mice also fed a HFD. The phenotypic similarity, together with the results of previous *in vitro* studies (2, 6, 7), strongly suggests that LKB1 is an upstream kinase of NUAK1 in skeletal muscle. Note that the phenotype of MNUAK1KO mice was apparent only under HFD conditions. This can be explained by the contribution of skeletal muscle to whole body glucose disposal. Under euglycemic conditions, the majority of glucose disposal occurs in a non-insulin-mediated manner, and skeletal muscle accounts for only 20% of whole body glucose disposal (47, 48). On the other hand, skeletal muscle is responsible for virtually all glucose disposal increased in hyperglycemic conditions (47). We concluded that a lack of NUAK1 alters muscle glucose metabolism, which contributes significantly to whole body glucose disposal in mice with hyperglycemia.

Our data provide evidence suggesting that NUAK1 controls glucose metabolism through negative regulation of insulin signal transduction in skeletal muscle. Firstly, the lower blood glucose of MNUAK1KO mice in OGTT and ITT indicates increased insulin sensitivity. Secondly, the *ex vivo* experiment of muscle glucose uptake suggests that NUAK1-deficient muscle is protected from HFD-induced insulin resistance. Thirdly, decreased phosphorylation of PKCθ at Ser-676 and IRS1 at Ser-1097 in the soleus muscle of MNUAK1KO mice indicates that a negative feedback regulation of insulin signal transduction is down-regulated by a lack of NUAK1. Indeed, phosphorylation of IRS1 at Tyr-608, which is caused by insulin and leads to the activation of downstream molecules such as AKT and TBC1D4, was up-regulated in the soleus muscle of MNUAK1KO mice. Our observations in MNUAK1KO mice are consistent with a report that PKCθ knock-out mice are not susceptible to HFD-induced insulin resistance (49). The hypophosphorylation of PKCθ in NUAK1-deficient soleus muscle also explains our observation that basal glucose uptake in muscle tended to be decreased by a lack of NUAK1 (Fig. 4, *A* and *B*), because it is regulated by PKC isoforms (50, 51). Lastly, increased muscle glycogen concentration together with decreased phosphorylation of GYS1 at Ser-653 and Ser-657, which is involved in activation of GYS1, can be explained by enhancement of insulin signaling because GYS1 at Ser-653 is regulated by glycogen synthase kinase 3, a downstream effector of IRS1-AKT axis (42).

How does NUAK1 control the negative feedback loop of insulin signaling? Phosphoproteome analysis showed that phosphorylation of IRS1 at Ser-1097 was decreased remarkably among all phosphorylations in soleus muscle. In adipose tissues, IRS1 is regulated by salt-inducible kinase 2, another member of the AMPK-RK family (52), through phosphorylation of Ser-794. Therefore, although the amino acid sequence flanking Ser-1097 is not consistent with the optimal motif for phosphorylation by AMPK (53–55), it is plausible that IRS1 is a target of NUAK1. The hypophosphorylation of PKCθ, an upstream kinase of IRS1 Ser-1097, can be explained by the lower plasma free fatty acid levels in MNUAK1KO mice because the phosphorylation of PKCθ is stimulated by free fatty acid (56–58).

Our phosphoproteome analysis also revealed that deletion of Nuak1 leads to a decrease in phosphorylation of components of contraction apparatus such as myosin isoforms and titin, which is consistent with a recent report suggesting that myosin and

paramyosin are potential substrates of UNC-82, a *Caenorhabditis elegans* ortholog of NUAK1 and NUAK2 (59). Current understanding of how changes in the phosphorylation status of cytoskeletal proteins affect glucose metabolism and muscle contraction is incomplete. Further phenotypic analyses of cytoskeletal organization and muscle contraction are required to fully understand the role of NUAK1 in skeletal muscle.

In summary, we found that NUAK1 is preferentially expressed in highly oxidative tissues such as the cerebrum, heart, and soleus muscle. We generated muscle-specific NUAK1 knock-out mice and found that they have improved glucose homeostasis compared with control mice when fed a hyperglycemia-inducing HFD. This phenotype is similar to that of muscle-specific LKB1 knock-out mice, suggesting that LKB1 is an upstream kinase for NUAK1 in skeletal muscle. A quantitative phosphoproteome analysis revealed that NUAK1 is involved in the negative feedback regulation of insulin signal transduction, possibly through the phosphorylation of IRS1. Our results strongly suggest that a physiological role of NUAK1 is to suppress insulin-mediated glucose uptake in skeletal muscle.

Acknowledgments—We thank Dr. Izumi O. Umeda and Dr. Hirofumi Fujii (Functional Imaging Division, Research Center for Innovative Oncology, National Cancer Center Hospital East, Kashiwa, Japan) for invaluable advice for the ex vivo glucose uptake experiment.

REFERENCES

1. Manning, G., Whyte, D. B., Martinez, R., Hunter, T., and Sudarsanam, S. (2002) The protein kinase complement of the human genome. *Science* **298,** 1912–1934
2. Lizcano, J. M., Göransson, O., Toth, R., Deak, M., Morrice, N. A., Boudeau, J., Hawley, S. A., Udd, L., Mäkelä, T. P., Hardie, D. G., and Alessi, D. R. (2004) LKB1 is a master kinase that activates 13 kinases of the AMPK subfamily, including MARK/PAR-1. *EMBO J.* **23,** 833–843
3. Scott, J. W., Ross, F. A., Liu, J. K., and Hardie, D. G. (2007) Regulation of AMP-activated protein kinase by a pseudosubstrate sequence on the γ subunit. *EMBO J.* **26,** 806–815
4. Al-Hakim, A. K., Göransson, O., Deak, M., Toth, R., Campbell, D. G., Morrice, N. A., Prescott, A. R., and Alessi, D. R. (2005) 14-3-3 cooperates with LKB1 to regulate the activity and localization of QSK and SIK. *J. Cell Sci.* **118,** 5661–5673
5. Suzuki, A., Kusakai, G., Kishimoto, A., Lu, J., Ogura, T., Lavin, M. F., and Esumi, H. (2003) Identification of a novel protein kinase mediating Akt survival signaling to the ATM protein. *J. Biol. Chem.* **278,** 48–53
6. Humbert, N., Navaratnam, N., Augert, A., Da Costa, M., Martien, S., Wang, J., Martinez, D., Abbadie, C., Carling, D., de Launoit, Y., Gil, J., and Bernard, D. (2010) Regulation of ploidy and senescence by the AMPK-related kinase NUAK1. *EMBO J.* **29,** 376–386
7. Zagórska, A., Deak, M., Campbell, D. G., Banerjee, S., Hirano, M., Aizawa, S., Prescott, A. R., and Alessi, D. R. (2010) New roles for the LKB1-NUAK pathway in controlling myosin phosphatase complexes and cell adhesion. *Sci. Signal.* **3,** ra25
8. Hou, X., Liu, J. E., Liu, W., Liu, C. Y., Liu, Z. Y., and Sun, Z. Y. (2011) A new role of NUAK1. Directly phosphorylating p53 and regulating cell proliferation. *Oncogene* **30,** 2933–2942
9. Niesler, C. U., Myburgh, K. H., and Moore, F. (2007) The changing AMPK expression profile in differentiating mouse skeletal muscle myoblast cells helps confer increasing resistance to apoptosis. *Exp. Physiol.* **92,** 207–217
10. Hirano, M., Kiyonari, H., Inoue, A., Furushima, K., Murata, T., Suda, Y., and Aizawa, S. (2006) A new serine/threonine protein kinase, Omphk1, essential to ventral body wall formation. *Dev. Dyn.* **235,** 2229–2237
11. Kusakai, G., Suzuki, A., Ogura, T., Kaminishi, M., and Esumi, H. (2004) Strong association of ARK5 with tumor invasion and metastasis. *J. Exp. Clin. Cancer Res.* **23,** 263–268
12. DeFronzo, R. A., Ferrannini, E., Sato, Y., Felig, P., and Wahren, J. (1981) Synergistic interaction between exercise and insulin on peripheral glucose uptake. *J. Clin. Invest.* **68,** 1468–1474
13. Goodyear, L. J., and Kahn, B. B. (1998) Exercise, glucose transport, and insulin sensitivity. *Annu. Rev. Med.* **49,** 235–261
14. Mu, J., Brozinick, J. T., Jr., Valladares, O., Bucan, M., and Birnbaum, M. J. (2001) A role for AMP-activated protein kinase in contraction- and hypoxia-regulated glucose transport in skeletal muscle. *Mol. Cell* **7,** 1085–1094
15. Jørgensen, S. B., Viollet, B., Andreelli, F., Frøsig, C., Birk, J. B., Schjerling, P., Vaulont, S., Richter, E. A., and Wojtaszewski, J. F. (2004) Knockout of the α2 but not α1 5′-AMP-activated protein kinase isoform abolishes 5-aminoimidazole-4-carboxamide-1-β-4-ribofuranoside but not contraction-induced glucose uptake in skeletal muscle. *J. Biol. Chem.* **279,** 1070–1079
16. Sakamoto, K., Göransson, O., Hardie, D. G., and Alessi, D. R. (2004) Activity of LKB1 and AMPK-related kinases in skeletal muscle. Effects of contraction, phenformin, and AICAR. *Am. J. Physiol. Endocrinol. Metab.* **287,** E310–E317
17. Hayashi, T., Hirshman, M. F., Kurth, E. J., Winder, W. W., and Goodyear, L. J. (1998) Evidence for 5′ AMP-activated protein kinase mediation of the effect of muscle contraction on glucose transport. *Diabetes* **47,** 1369–1373
18. Sakamoto, K., McCarthy, A., Smith, D., Green, K. A., Grahame Hardie, D., Ashworth, A., and Alessi, D. R. (2005) Deficiency of LKB1 in skeletal muscle prevents AMPK activation and glucose uptake during contraction. *EMBO J.* **24,** 1810–1820
19. Fujii, N., Hirshman, M. F., Kane, E. M., Ho, R. C., Peter, L. E., Seifert, M. M., and Goodyear, L. J. (2005) AMP-activated protein kinase α2 activity is not essential for contraction- and hyperosmolarity-induced glucose transport in skeletal muscle. *J. Biol. Chem.* **280,** 39033–39041
20. Koh, H. J., Toyoda, T., Fujii, N., Jung, M. M., Rathod, A., Middelbeek, R. J., Lessard, S. J., Treebak, J. T., Tsuchihara, K., Esumi, H., Richter, E. A., Wojtaszewski, J. F., Hirshman, M. F., and Goodyear, L. J. (2010) Sucrose nonfermenting AMPK-related kinase (SNARK) mediates contraction-stimulated glucose transport in mouse skeletal muscle. *Proc. Natl. Acad. Sci. U.S.A.* **107,** 15541–15546
21. Koh, H. J., Arnolds, D. E., Fujii, N., Tran, T. T., Rogers, M. J., Jessen, N., Li, Y., Liew, C. W., Ho, R. C., Hirshman, M. F., Kulkarni, R. N., Kahn, C. R., and Goodyear, L. J. (2006) Skeletal muscle-selective knockout of LKB1 increases insulin sensitivity, improves glucose homeostasis, and decreases TRB3. *Mol. Cell Biol.* **26,** 8217–8227
22. Fujii, N., Ho, R. C., Manabe, Y., Jessen, N., Toyoda, T., Holland, W. L., Summers, S. A., Hirshman, M. F., and Goodyear, L. J. (2008) Ablation of AMP-activated protein kinase α2 activity exacerbates insulin resistance induced by high-fat feeding of mice. *Diabetes* **57,** 2958–2966
23. Alkhateeb, H., Chabowski, A., Glatz, J. F., Luiken, J. F., and Bonen, A. (2007) Two phases of palmitate-induced insulin resistance in skeletal muscle. Impaired GLUT4 translocation is followed by a reduced GLUT4 intrinsic activity. *Am. J. Physiol. Endocrinol. Metab.* **293,** E783–E793
24. Saito, H., Oda, Y., Sato, T., Kuromitsu, J., and Ishihama, Y. (2006) Multiplexed two-dimensional liquid chromatography for MALDI and nano-electrospray ionization mass spectrometry in proteomics. *J. Proteome Res.* **5,** 1803–1807
25. Rappsilber, J., Ishihama, Y., and Mann, M. (2003) Stop and go extraction tips for matrix-assisted laser desorption/ionization, nanoelectrospray, and LC/MS sample pretreatment in proteomics. *Anal. Chem.* **75,** 663–670
26. Boersema, P. J., Raijmakers, R., Lemeer, S., Mohammed, S., and Heck, A. J. (2009) Multiplex peptide stable isotope dimethyl labeling for quantitative proteomics. *Nat. Protoc.* **4,** 484–494
27. Sugiyama, N., Masuda, T., Shinoda, K., Nakamura, A., Tomita, M., and Ishihama, Y. (2007) Phosphopeptide enrichment by aliphatic hydroxy acid-modified metal oxide chromatography for nano-LC-MS/MS in proteomics applications. *Mol. Cell. Proteomics* **6,** 1103–1109
28. Nakagami, H., Sugiyama, N., Mochida, K., Daudi, A., Yoshida, Y., Toyoda, T., Tomita, M., Ishihama, Y., and Shirasu, K. (2010) Large-scale compar-

ative phosphoproteomics identifies conserved phosphorylation sites in plants. *Plant Physiol.* **153,** 1161–1174
29. Mann, M., and Wilm, M. (1994) Error-tolerant identification of peptides in sequence databases by peptide sequence tags. *Anal. Chem.* **66,** 4390–4399
30. Yamamoto, H., Takashima, S., Shintani, Y., Yamazaki, S., Seguchi, O., Nakano, A., Higo, S., Kato, H., Liao, Y., Asano, Y., Minamino, T., Matsumura, Y., Takeda, H., and Kitakaze, M. (2008) Identification of a novel substrate for TNFα-induced kinase NUAK2. *Biochem. Biophys. Res. Commun.* **365,** 541–547
31. Nagase, T., Ishikawa, K., Miyajima, N., Tanaka, A., Kotani, H., Nomura, N., and Ohara, O. (1998) Prediction of the coding sequences of unidentified human genes. IX. The complete sequences of 100 new cDNA clones from brain which can code for large proteins in vitro. *DNA Res.* **5,** 31–39
32. Bassel-Duby, R., and Olson, E. N. (2006) Signaling pathways in skeletal muscle remodeling. *Annu. Rev. Biochem.* **75,** 19–37
33. Lin, J., Wu, H., Tarr, P. T., Zhang, C. Y., Wu, Z., Boss, O., Michael, L. F., Puigserver, P., Isotani, E., Olson, E. N., Lowell, B. B., Bassel-Duby, R., and Spiegelman, B. M. (2002) Transcriptional co-activator PGC-1α drives the formation of slow-twitch muscle fibres. *Nature* **418,** 797–801
34. McGee, S. L., Sparling, D., Olson, A. L., and Hargreaves, M. (2006) Exercise increases MEF2- and GEF DNA-binding activity in human skeletal muscle. *FASEB J.* **20,** 348–349
35. Kim, Y., Tamura, T., Iwashita, S., Tokuyama, K., and Suzuki, M. (1994) Effect of high-fat diet on gene expression of GLUT4 and insulin receptor in soleus muscle. *Biochem. Biophys. Res. Commun.* **202,** 519–526
36. Tsao, T. S., Stenbit, A. E., Factor, S. M., Chen, W., Rossetti, L., and Charron, M. J. (1999) Prevention of insulin resistance and diabetes in mice heterozygous for GLUT4 ablation by transgenic complementation of GLUT4 in skeletal muscle. *Diabetes* **48,** 775–782
37. Treadway, J. L., Hargrove, D. M., Nardone, N. A., McPherson, R. K., Russo, J. F., Milici, A. J., Stukenbrok, H. A., Gibbs, E. M., Stevenson, R. W., and Pessin, J. E. (1994) Enhanced peripheral glucose utilization in transgenic mice expressing the human GLUT4 gene. *J. Biol. Chem.* **269,** 29956–29961
38. Garvey, W. T., Maianu, L., Zhu, J. H., Brechtel-Hook, G., Wallace, P., and Baron, A. D. (1998) Evidence for defects in the trafficking and translocation of GLUT4 glucose transporters in skeletal muscle as a cause of human insulin resistance. *J. Clin. Invest.* **101,** 2377–2386
39. Kramer, H. F., Witczak, C. A., Taylor, E. B., Fujii, N., Hirshman, M. F., and Goodyear, L. J. (2006) AS160 regulates insulin- and contraction-stimulated glucose uptake in mouse skeletal muscle. *J. Biol. Chem.* **281,** 31478–31485
40. Thong, F. S., Bilan, P. J., and Klip, A. (2007) The Rab GTPase-activating protein AS160 integrates Akt, protein kinase C, and AMP-activated protein kinase signals regulating GLUT4 traffic. *Diabetes* **56,** 414–423
41. Li, Y., Soos, T. J., Li, X., Wu, J., Degennaro, M., Sun, X., Littman, D. R., Birnbaum, M. J., and Polakiewicz, R. D. (2004) Protein kinase Cθ inhibits insulin signaling by phosphorylating IRS1 at Ser^{1101}. *J. Biol. Chem.* **279,** 45304–45307
42. Roach, P. J. (1990) Control of glycogen synthase by hierarchal protein phosphorylation. *FASEB J.* **4,** 2961–2968
43. Fiol, C. J., Mahrenholz, A. M., Wang, Y., Roeske, R. W., and Roach, P. J. (1987) Formation of protein kinase recognition sites by covalent modification of the substrate. Molecular mechanism for the synergistic action of casein kinase II and glycogen synthase kinase 3. *J. Biol. Chem.* **262,** 14042–14048
44. Khamzina, L., Veilleux, A., Bergeron, S., and Marette, A. (2005) Increased activation of the mammalian target of rapamycin pathway in liver and skeletal muscle of obese rats. Possible involvement in obesity-linked insulin resistance. *Endocrinology* **146,** 1473–1481
45. Liu, H. Y., Hong, T., Wen, G. B., Han, J., Zuo, D., Liu, Z., and Cao, W. (2009) Increased basal level of Akt-dependent insulin signaling may be responsible for the development of insulin resistance. *Am. J. Physiol. Endocrinol. Metab.* **297,** E898–E906
46. Richardson, J. M., Balon, T. W., Treadway, J. L., and Pessin, J. E. (1991) Differential regulation of glucose transporter activity and expression in red and white skeletal muscle. *J. Biol. Chem.* **266,** 12690–12694
47. Baron, A. D., Brechtel, G., Wallace, P., and Edelman, S. V. (1988) Rates and tissue sites of non-insulin- and insulin-mediated glucose uptake in humans. *Am. J. Physiol.* **255,** E769–E774
48. Lang, C. H. (1992) Rates and tissue sites of noninsulin- and insulin-mediated glucose uptake in diabetic rats. *Proc. Soc. Exp. Biol. Med.* **199,** 81–87
49. Kim, J. K., Fillmore, J. J., Sunshine, M. J., Albrecht, B., Higashimori, T., Kim, D. W., Liu, Z. X., Soos, T. J., Cline, G. W., O'Brien, W. R., Littman, D. R., and Shulman, G. I. (2004) PKC-θ knockout mice are protected from fat-induced insulin resistance. *J. Clin. Invest.* **114,** 823–827
50. Shillabeer, G., Chamoun, C., Hatch, G., and Lau, D. C. (1995) Exogenous triacylglycerol inhibits insulin-stimulated glucose transport in L6 muscle cells *in vitro*. *Biochem. Biophys. Res. Commun.* **207,** 768–774
51. Montell, E., Turini, M., Marotta, M., Roberts, M., Noé, V., Ciudad, C. J., Macé, K., and Gómez-Foix, A. M. (2001) DAG accumulation from saturated fatty acids desensitizes insulin stimulation of glucose uptake in muscle cells. *Am. J. Physiol. Endocrinol. Metab.* **280,** E229–E237
52. Horike, N., Takemori, H., Katoh, Y., Doi, J., Min, L., Asano, T., Sun, X. J., Yamamoto, H., Kasayama, S., Muraoka, M., Nonaka, Y., and Okamoto, M. (2003) Adipose-specific expression, phosphorylation of Ser^{794} in insulin receptor substrate-1, and activation in diabetic animals of salt-inducible kinase-2. *J. Biol. Chem.* **278,** 18440–18447
53. Dale, S., Wilson, W. A., Edelman, A. M., and Hardie, D. G. (1995) Similar substrate recognition motifs for mammalian AMP-activated protein kinase, higher plant HMG-CoA reductase kinase-A, yeast SNF1, and mammalian calmodulin-dependent protein kinase I. *FEBS Lett.* **361,** 191–195
54. Scott, J. W., Norman, D. G., Hawley, S. A., Kontogiannis, L., and Hardie, D. G. (2002) Protein kinase substrate recognition studied using the recombinant catalytic domain of AMP-activated protein kinase and a model substrate. *J. Mol. Biol.* **317,** 309–323
55. Gwinn, D. M., Shackelford, D. B., Egan, D. F., Mihaylova, M. M., Mery, A., Vasquez, D. S., Turk, B. E., and Shaw, R. J. (2008) AMPK phosphorylation of raptor mediates a metabolic checkpoint. *Mol. Cell* **30,** 214–226
56. Qu, X., Seale, J. P., and Donnelly, R. (1999) Tissue and isoform-selective activation of protein kinase C in insulin-resistant obese Zucker rats. Effects of feeding. *J. Endocrinol.* **162,** 207–214
57. Itani, S. I., Pories, W. J., Macdonald, K. G., and Dohm, G. L. (2001) Increased protein kinase Cθ in skeletal muscle of diabetic patients. *Metabolism* **50,** 553–557
58. Griffin, M. E., Marcucci, M. J., Cline, G. W., Bell, K., Barucci, N., Lee, D., Goodyear, L. J., Kraegen, E. W., White, M. F., and Shulman, G. I. (1999) Free fatty acid-induced insulin resistance is associated with activation of protein kinase Cθ and alterations in the insulin signaling cascade. *Diabetes* **48,** 1270–1274
59. Hoppe, P. E., Chau, J., Flanagan, K. A., Reedy, A. R., and Schriefer, L. A. (2010) *Caenorhabditis elegans* unc-82 encodes a serine/threonine kinase important for myosin filament organization in muscle during growth. *Genetics* **184,** 79–90

DOI: 10.1002/cmdc.201100564

Synthesis and Evaluation of Anticancer Natural Product Analogues Based on Angelmarin: Targeting the Tolerance towards Nutrient Deprivation

Jakob Magolan,[a] Nathan B. P. Adams,[a] Hiroko Onozuka,[b] Natasha L. Hungerford,[a] Hiroyasu Esumi,[b] and Mark J. Coster*[a]

Rapidly growing solid tumours are often inherently hypovascular, thus exhibiting reduced oxygen and nutrient supply.[1–2] This has been well documented in pancreatic tumours.[3–5] Rather than impeding cancer progression, such poor metabolic conditions can contribute to genomic instability, impaired cellular repair, mutagenesis, and resistance to chemotherapy, thus worsening prognoses for patients.[6–9]

The therapeutic strategies of angiogenesis inhibition[10,11] and vascular targeting[12] endeavour to kill tumour cells by selectively depriving them of oxygen and nutrients. In this light, aggressive tumours that thrive despite being chronically hypoxic and nutrient-deprived present a serious therapeutic challenge■ ■ok?■ ■. Despite considerable evidence of angiogenesis,[13–17] many pancreatic tumours remain hypovascular, hypoxic, and starved of nutrients while continuing to grow rapidly.

In 2000, Esumi and co-workers showed conclusively that certain pancreatic cancer cell lines, in contrast to other cancer cell lines and normal human fibroblasts, demonstrate an extraordinary capacity for survival in nutrient-deprived medium (NDM).[18] The specific biochemical mechanisms associated with starvation resistance, termed austerity, continue to be elucidated.[19]

Concurrently, a screening method for antiausterity activity has been developed,[20] and a number of small-molecule inhibitors of this process—antiausterity agents—have recently been identified.[19] Furthermore, three of these antiausterity agents have been shown in vivo to slow the growth of xenograft tumours of of PANC-1, a human pancreatic carcinoma, epithelial-like cell line■ ■ok?■ ■.[20–22] Subsequent to our recent comparative review of known antiausterity agents,[19] the first simplified natural product analogues with modest antiausterity activity have been described.[23,24]

During their extensive discovery efforts using antiausterity bioassay-guided fractionation of plant extracts,[25–33] Awale, Kadota and co-workers isolated (+)-angelmarin from *Angelica pubescens*, finding it to have preferential cytotoxicity (PC; see below for definition■ ■ok?■ ■) towards PANC-1 cells in NDM (24 hour incubation) at a concentration of 0.01 μg mL^{-1} (PC_{100} = 26 nM), with no cytotoxicity in nutrient-rich medium.[25]

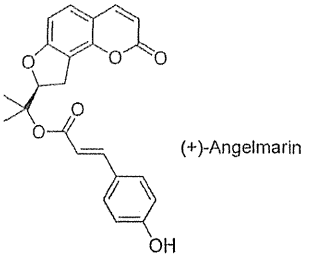

In 2009, we disclosed an enantioselective synthesis of (+)-angelmarin.[34] Total syntheses of this target compound have also been recently reported by Hamada[35] and Banwell.[36] Herein, we provide results of ongoing structure–activity relationship (SAR) investigations into this natural product, with the long-term aim to gain sufficient insight for the development of probes to study the mechanism of action and to elucidate the biological target(s) for antiausterity.

Our eight-step synthetic sequence afforded (+)-angelmarin in 37% overall yield and 75% enantiomeric exces (*ee*) from commercially available umbelliferone.[34] The racemate was also prepared in six steps in 48% overall yield, as shown in Scheme 1.[34] Allylation of umbelliferone, followed by Claisen rearrangement yielded **2**.[37] Cross metathesis of terminal olefin **2** and 2-methyl-2-butene in the presence of Grubbs' second-generation catalyst provided osthenol (**3**). Epoxidation with *meta*-chloroperoxybenzoic acid (*m*-CPBA) in the presence of potassium carbonate readily yielded *rac*-columbianetin (**4**). Treatment with 2,2-dimethyl-1,3-dioxane-4,6-dione (Meldrum's acid)■ ■ok?■ ■ in refluxing toluene provided carboxylic acid **5**, which was converted to (±)-angelmarin (**6**) via a Doebner–Knoevanagel condensation, by heating the substrate in the presence of 4-hydroxybenzaldehyde and piperidine in pyridine (82% yield, over two steps).

The final step of this sequence was readily amenable to divergent analogue synthesis using alternate aldehydes ■ ■(**7**)? ■ ■. In this manner, 20 racemic angelmarin analogues (**8a–t**) were prepared as illustrated in Scheme 2. Columbianetin acetate (**9**) was obtained as a minor by-product (0–35 mol%) of this reaction.[38]

Two additional analogues, 2′,3′-dihydroangelmarin **10** and 3,4,2′,3′-tetrahydroangelmarin **11** were readily prepared via hydrogenation of (±)-angelmarin (**6**) over $Pt(OH)_2$ and Pd/C, respectively (Scheme 3).

To further examine the importance of the cinnamate subunit, carbamate **13** was prepared. Treatment of (±)-columbianetin **4** with triphosgene[39,40] in the presence of 4-dimethylami-

[a] *Dr. J. Magolan, N. B. P. Adams, Dr. N. L. Hungerford, Dr. M. J. Coster*
Eskitis Institute for Cell and Molecular Therapies (N75)
Griffith University, Nathan Campus
Brisbane Innovation Park, Don Young Road, Nathan, QLD 4111 (Australia)
Fax: (+61) 7 3735 6001
E-mail: m.coster@griffith.edu.au

[b] *H. Onozuka, Prof. H. Esumi*
Cancer Physiology Project, Research Center for Innovative Oncology
National Cancer Center Hospital East
6-5-1 Kashiwanoha, Kashiwa, Chiba 277-8577 (Japan)

Supporting information for this article is available on the WWW under http://dx.doi.org/10.1002/cmdc.201100564.

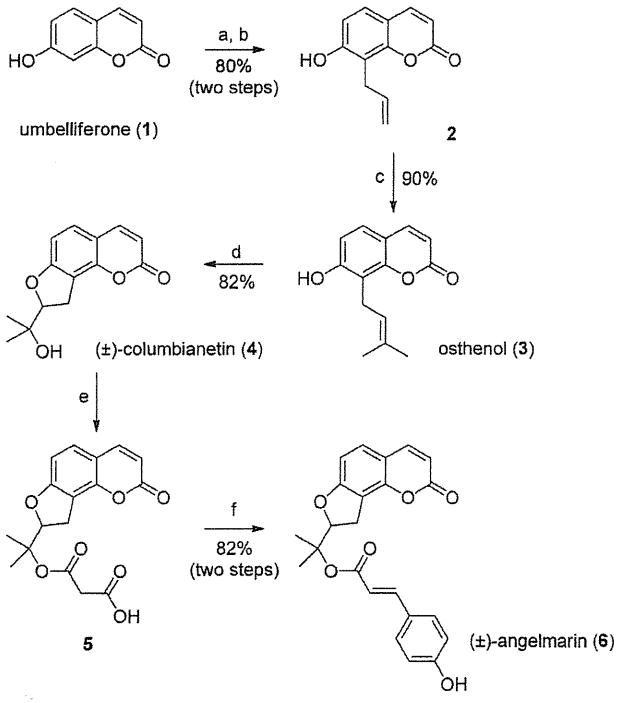

Scheme 1. Synthesis of (±)-angelmarin (**6**). *Reagents and conditions*: a) Allyl bromide, K_2CO_3, acetone, reflux, 6 h; b) $PhNEt_2$, reflux, 4 h; c) Grubbs II, 2-methyl-2-butene, CH_2Cl_2, reflux (slow addition of substrate); d) *m*-CPBA, K_2CO_3, CH_2Cl_2, RT, 8 h; e) Meldrum's acid, toluene, reflux, 6 h; f) 4-hydroxybenzaldehyde, piperidine, pyridine, 70 °C, 12 h.

nopyridine (DMAP) gave reactive intermediate chloroformate **12**. It should be noted that safe handling procedures should be observed when using triphosgene.[41] Finally, addition of benzylamine to the chloroformate **12**, in situ, afforded carbamate **13** (Scheme 4).

In a preliminary effort to gauge the biological significance of the coumarin portion of the natural product, analogue **15** was prepared in two steps from dihydrobenzofuran tertiary alcohol **14**, as shown in Scheme 5.

In contrast to conventional anticancer activity, an inhibitor of the austerity pathway is cytotoxic to starvation-resistant cancer cells only under nutrient-deprived conditions. This anti-austerity activity can be quantified in terms of preferential cytotoxicity (PC). The evaluation is conducted using two assays in parallel, with PANC-1 cells in both nutrient-rich, such as Dulbecco's modified Eagle medium (DMEM), and NDM. The PC_{50} value is defined as the IC_{50} of a compound in NDM, where the compound is not cytotoxic in nutrient-rich medium. Synthetic angelmarin analogues were tested in vitro for preferential cytotoxicity against PANC-1 cells cultured in NDM.[20] These analogues exhibited a range of preferential cytotoxic potencies as shown in Table 1.

Racemic angelmarin (**6**) exhibits a PC_{50} value of 91 nM (c.f., PC_{100} value of 26 nM obtained for the plant-derived (+)-enantiomer in the laboratories of Kadota et al.[25]). Our initial SAR investigations involved the replacement of the *para*-hydroxy substituent of (±)-angelmarin (**6**) with a variety of other groups (**8a–k**). Removal of the phenolic hydroxy group did not

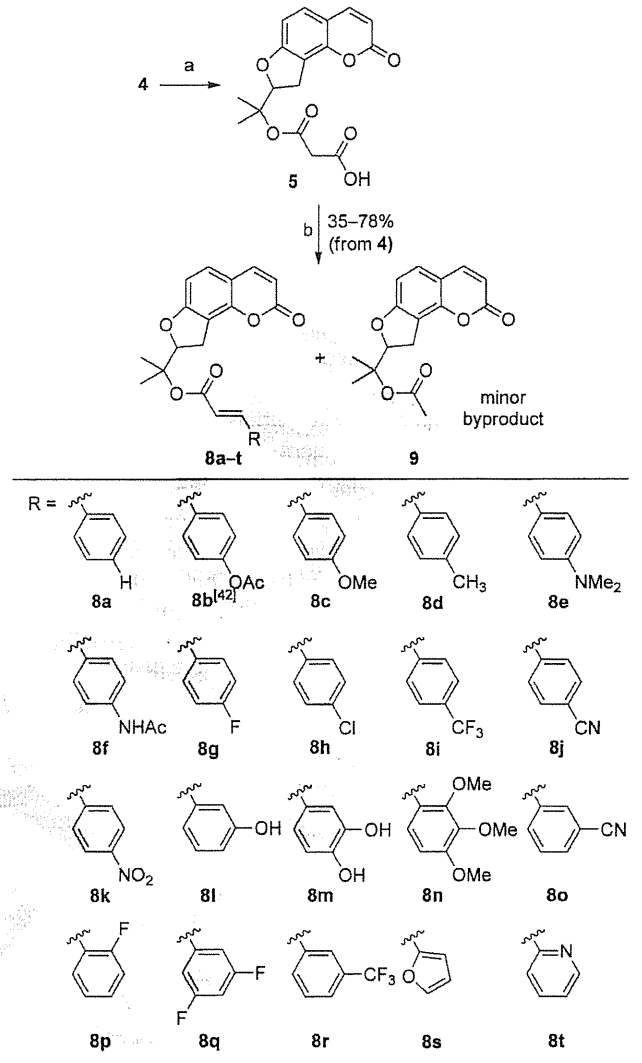

Scheme 2. Synthesis of angelmarin analogues **8a–t**. *Reagents and conditions*: a) Meldrum's acid, toluene, reflux, 7 h; b) carboxylic acid **5**, RCHO **7**, piperidine, pyridine, 70 °C, 12 h.

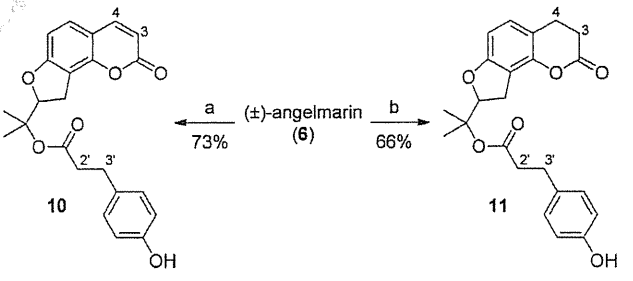

Scheme 3. Hydrogenation of (±)-angelmarin (**6**) to yield compounds **10** and **11**. *Reagents and conditions*: a) H_2 (1 atm), $Pt(OH)_2$,THF, RT, 4 h; b) H_2 (1 atm), Pd/C, EtOAc, RT, 16 h.

entirely eliminate the cytotoxicity of the resultant compound (**8a**), but rather led to a threefold decrease in activity. In contrast, conversion of the phenol group in **6** to the corresponding acetate ester to give compound **8b**[42] resulted in a ninefold increase in preferential cytotoxicity (PC_{50} = 10 nM). Ester **8b**

